

1 Sensing Performance of Gas Sensors Fabricated from Controllably 2 Grown ZnO-Based Nanorods on Seed Layers

3 Pragya Singh¹, Firman Mangasa Simanjuntak², Yi-Chu Wu³, Amit Kumar⁴, Hsiao-Wen Zan^{3*},
4 Tseung-Yuen Tseng^{4*}

5 ¹ *Department of Electrical Engineering and Computer Science, National Chiao Tung University,*
6 *Hsinchu 30010, Taiwan*

7 ² *Zepler Institute of Photonics and Electronics, University of Southampton, Southampton SO17*
8 *1BJ, United Kingdom*

9 ³ *Department of Photonics and Institute of Electro-Optical Engineering, National Chiao Tung*
10 *University, Hsinchu 30010, Taiwan*

11 ⁴ *Institute of Electronics, National Chiao Tung University, Hsinchu 30010, Taiwan*

12 * Corresponding authors email: tseng@cc.nctu.edu.tw, hsiaowen@mail.nctu.edu.tw

14 **ABSTRACT**

15 ZnO nanorods (NRs) grown on different ZnO seed layers deposited at various Ar–O₂ ambient
16 conditions and the morphologies of the seed layers that affect their response to nitric oxide (NO)
17 gas were investigated. The sensing performance of the devices fabricated with the seed layers
18 deposited under an O₂-rich condition tends to deteriorate. We believe that the surface roughness,
19 grain size, and defect concentration of the seed layer are responsible for this phenomenon. Despite
20 the response to the gas was found to be less dependent on NR length, the gas sensing response is
21 significantly dependent on the oxygen vacancy concentration and the exposure of the NR structure
22 to the NO gas ambient surface. Excellent gas response (57.5% at 1 ppm and 7.1% at 100 ppb of
23 NO gas) was achieved at room temperature—superior to the response presented by other proposed
24 methods. This study not only proposes the potential of ZnO-NRs for high-performance NO gas
25 sensor devices but also offers a simple and low-cost method to optimize the response without using
26 any catalyst and additional treatment.

27 *Keywords:* gas sensor device, NO gas sensing, hydrothermal growth, ZnO, nanorod.

28

29 **Introduction**

30 Nitric oxide (NO) is a common air pollutant that is exhausted by car engines, boilers, and other
31 combustion processes on a daily basis [1]. Inhalation of NO gas causes detrimental functional
32 changes in the lungs, causes asthma, degrades the immune system, and facilitates blood-borne
33 cancer cell metastasis [2,3]. Therefore, designing reliable and highly responsive NO gas sensor
34 devices to monitor NO leakage to the environment is crucial.

35 Numerous designs of NO gas sensors employing ZnO oxides have been proposed [4,5].
36 ZnO is mostly used as a gas-sensing material because of its high sensitivity, low-temperature
37 fabrication, low cost, and environment friendliness, excellent chemical and thermal stability, and
38 unique ability to form one-dimensional (1D) nanostructures [6]. The employment of 1D
39 nanostructures [e.g., nanorods (NRs), nanocombs, nanotetrapods, and nanobelts improves the gas-
40 sensing performance [7,8]. In particular, ZnO-NRs reveal a high surface to volume ratio that
41 enables the exchange of charge carriers during the oxidation–reduction mechanism and enables
42 rapid electron transport along the NRs that greatly enhance the charge concentration [11].

43 The hydrothermal growth technique is a solution-based process used to synthesize ZnO-
44 NRs, which has several advantages such as easy fabrication, low cost, and environment friendly
45 processes, that is beneficial for mass production [10,11]. Various techniques have been explored
46 for enhancing the sensing performance of ZnO-NR sensor devices, such as dopant addition [12,13],
47 quantum dot use [14], annealing [15], and UV light treatment [16]. Despite these proposed
48 techniques being able to enhance the sensing performance, we argue that suitable optimization of
49 the ZnO-NR growth should be considered before employing these techniques; by considering that
50 all the proposed techniques are expensive and time-consuming. Moreover, an effortless method
51 for fabricating a high-performance gas sensor without using a catalyst and without involving any

52 additional treatment is urgently required to significantly reduce the processing time and cost as
53 well as to encourage the realization of ZnO-based sensors for use in future sensing devices.

54 The hydrothermal growth technique requires a seed layer to provide ZnO nucleation sites
55 during the growth of the ZnO-NRs. Consequently, the properties of the seed layer defines NR
56 morphology in terms of the diameter, length, density, and alignment [10,17–21]. Thus, a fine
57 tuning on the seed layer is crucial for determining the sensing behavior of the devices. However,
58 the importance of the seed layer to the sensing performance is still overlooked. In this study, we
59 studied the morphology of the ZnO-NRs grown on sputtered seed layers that are deposited at
60 various gas ambient conditions, and the influence of such a modification on the sensing
61 performance of the ZnO-NRs was investigated.

62

63 **Experimental Method**

64 **Sensor device fabrication**

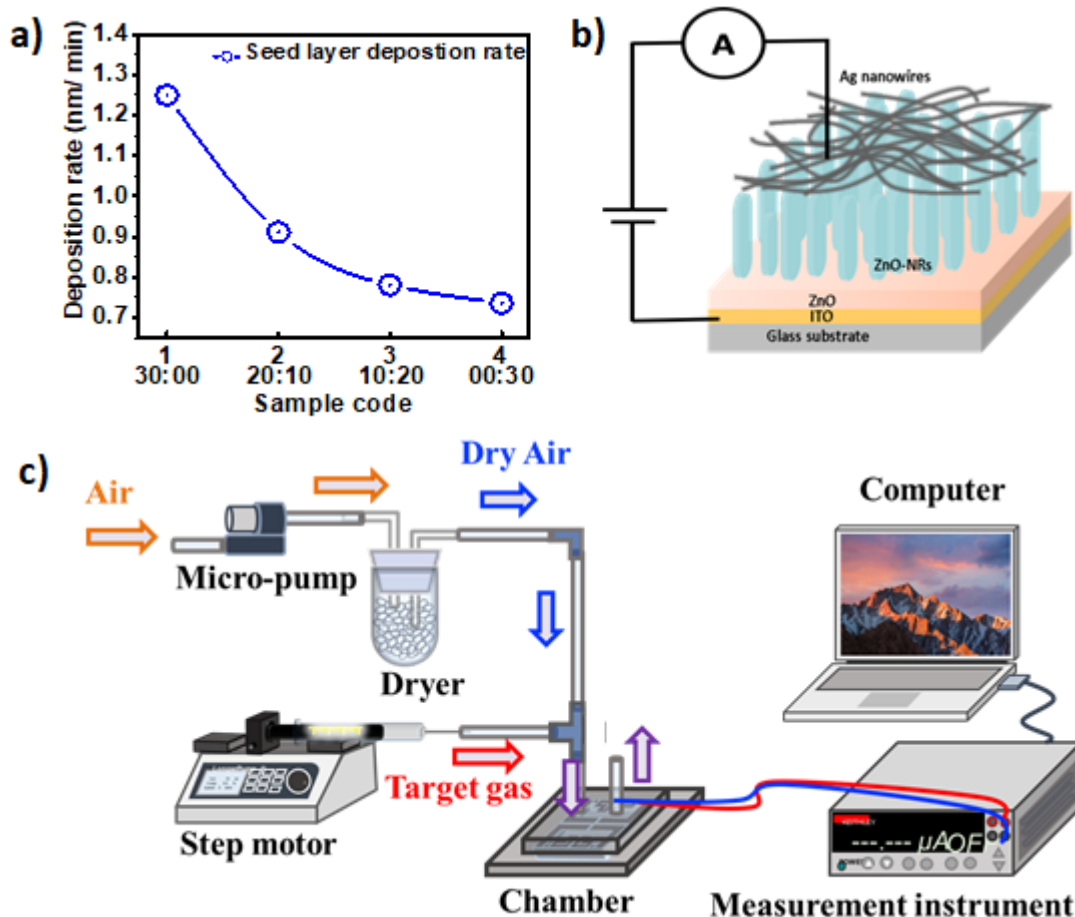
65 Approximately 260-nm-thick indium–tin–oxide (ITO)-coated glass substrates were cleaned using
66 acetone and DI water for 10 min. Then, ZnO seed layers were deposited on the ITO-substrates by
67 using radio-frequency magnetron sputtering at room temperature at various Ar–O₂ gas ratio
68 ambient conditions. The Ar–O₂ gas ratios employed are 1, 0.67, 0.33, and 1 with a flow rate of
69 30:00, 20:10, 10:20, and 00:30 sccm, respectively. The total gas flow was maintained at 30 sccm.
70 Deposition time was carefully controlled to fabricate the seed layer with a thickness of 50 nm. The
71 deposition rate of the ZnO seed layer at various gas ratio conditions is presented in Fig. 1(a). Then,
72 the ZnO-NRs were synthesized on the ZnO seed layer by employing a precursor aqueous solution
73 of zinc chloride (ZnCl₂) and ammonium hydroxide (NH₃OH), and the hydrothermal process was
74 maintained at 95°C for 10 min. The hydrothermal growth procedure adopted the method that was
75 explained in our previous studies [11,22]. To fabricate the top electrode, drop- cast method is used,

76 and silver nanowires dispensed in isopropanol (IPA) with concentration as 0.5 wt%. The average
77 diameter of silver nanowire is about 12–15 nm and an average length is about 80 nm. Silver (Ag)
78 nanowires were dropped on top of the active areas of the ZnO-NRs. A 40-nm-thick Al film was
79 deposited as an auxiliary electrode by using a thermal evaporator. The schematic of the fabricated
80 device is illustrated in Fig. 1(b). The devices, seed layers, and NRs are denoted as Dx, SLx, and
81 NRx, respectively. Here, x is denoted as 1, 2, 3, and 4. These values represent the gas ambient (Ar:
82 O₂) flow of 30:00, 20:10, 10:20, and 00:30 sccm, respectively, for the sputtered seed layer.

83

84 **Response measurement set-up**

85 The schematic of the gas-sensing measurement setup is shown in Fig. 1(c). An electrical syringe
86 pump was used to inject the target gas (NO, purity 99.999%) into a tube to mix the gas with the
87 background dry ambient air. The gas mixture then entered the microfluid system. The background
88 air was passed into the detection chamber. A moisture absorber (dryer) was first used to filter out
89 the water in the air. The air in the system was controlled in a low-humidity environment with a
90 relative humidity of 10% to prevent the components from being affected by room humidity
91 fluctuations. The current values of the ZnO-NR devices were measured using an electrical
92 measurement system (model 2400, Keithley Source Meter). The measurement setup was adopted
93 from a previous study [23].



94

95 **Fig 1.** (a) Deposition rate of the ZnO seed layer grown in various ambient conditions. (b)
 96 Schematic of the fabricated device (AgNWs/ZnO-NRs/ZnO/ITO/glass substrate). (c) Gas-sensing
 97 measurement system.

98

99 **Material analysis**

100 The morphology of the ZnO-NRs was examined by using scanning electron microscopy (SEM;
 101 Hitachi SU8010). The crystal structures of the ZnO-NRs and the seed layers were investigated
 102 through X-ray diffractometry (XRD; D1. Bede Plc.). The X-ray source is Cu K-alpha 1.5406 Å.
 103 The defect concentrations in the ZnO-NRs and the seed layer were evaluated using an X-ray

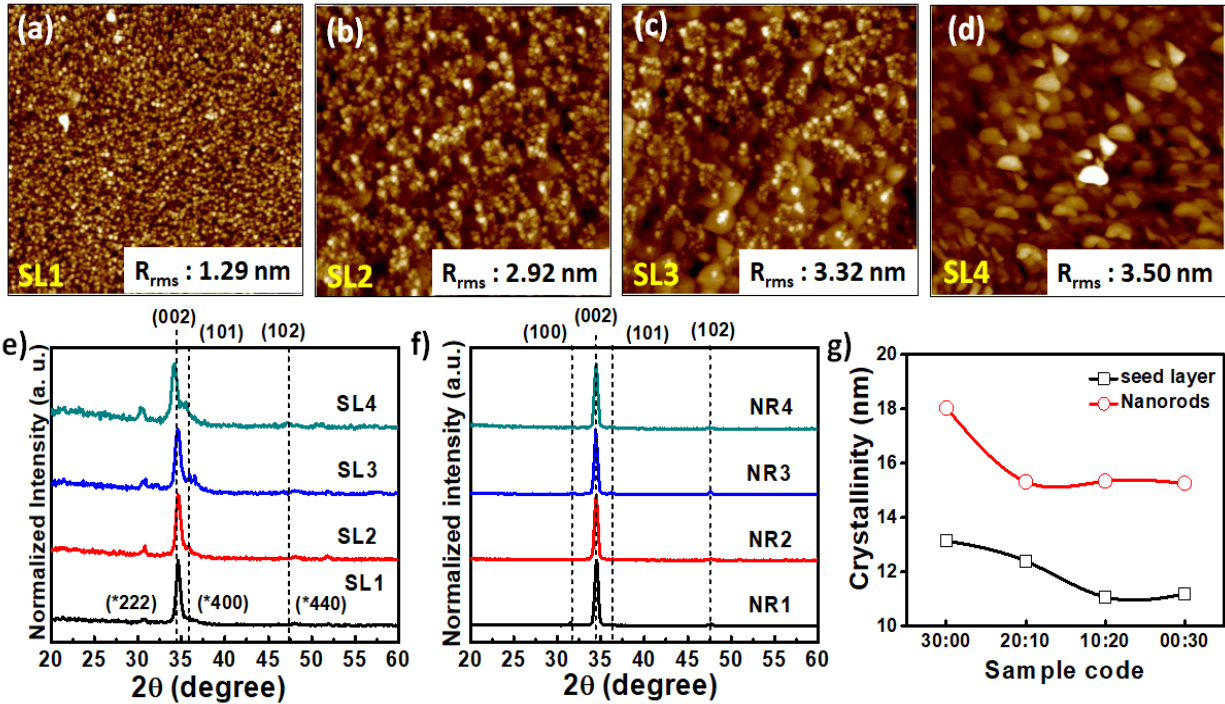
104 photoelectron spectroscopy (XPS; PHI Quantera SXM). A C1s peak with a binding energy of
105 284.5 eV was taken as a reference.

106

107 **Results and discussion**

108 **Effect of seed layer on ZnO NRs morphology**

109 The surface roughness of the seed layer serves a significant role in the ZnO-NR growth. Therefore,
110 the topography of the ZnO seed layer deposited at various Ar–O₂ gas ratios was obtained, and the
111 result are depicted in Figs. 2(a)–2(d). The surface roughness of the seed layer increases as the O₂
112 portion increases. This is due to the higher energetic bombardments of the oxygen ions on the
113 growth films, thus resulting in surface degradation [24]. Figures 2(e) and (f) present the XRD
114 patterns of the ZnO seed layer (ZnO-SL) grown at various Ar–O₂ gas ratios and the related ZnO-
115 NRs, respectively. The crystal structure of the ZnO-SL and ZnO-NRs is a hexagonal wurtzite
116 structure and reveals a preferred orientation of (002) (JCPDS, No. 36-1451). The grains of the seed
117 layer that grows in the (002) direction is beneficial in terms of the nucleation sites for NR growth
118 [17,25]. Therefore, the (002) grain size was calculated using the Scherer equation [26], and the
119 result is shown in Fig. 2(g). The grain size of (002) of the ZnO-SL decreases after introducing O₂
120 gas. The introduction of the neutral oxygen atoms enhances the growth of the grains in various
121 directions (Fig. 2(e)). Thus, the grain size of the (002) grains decreases due to the growth
122 competition process [27,28]. Consequently, the grain size of the NRs grown on the corresponding
123 seed layer decreases (Fig. 2(g)).



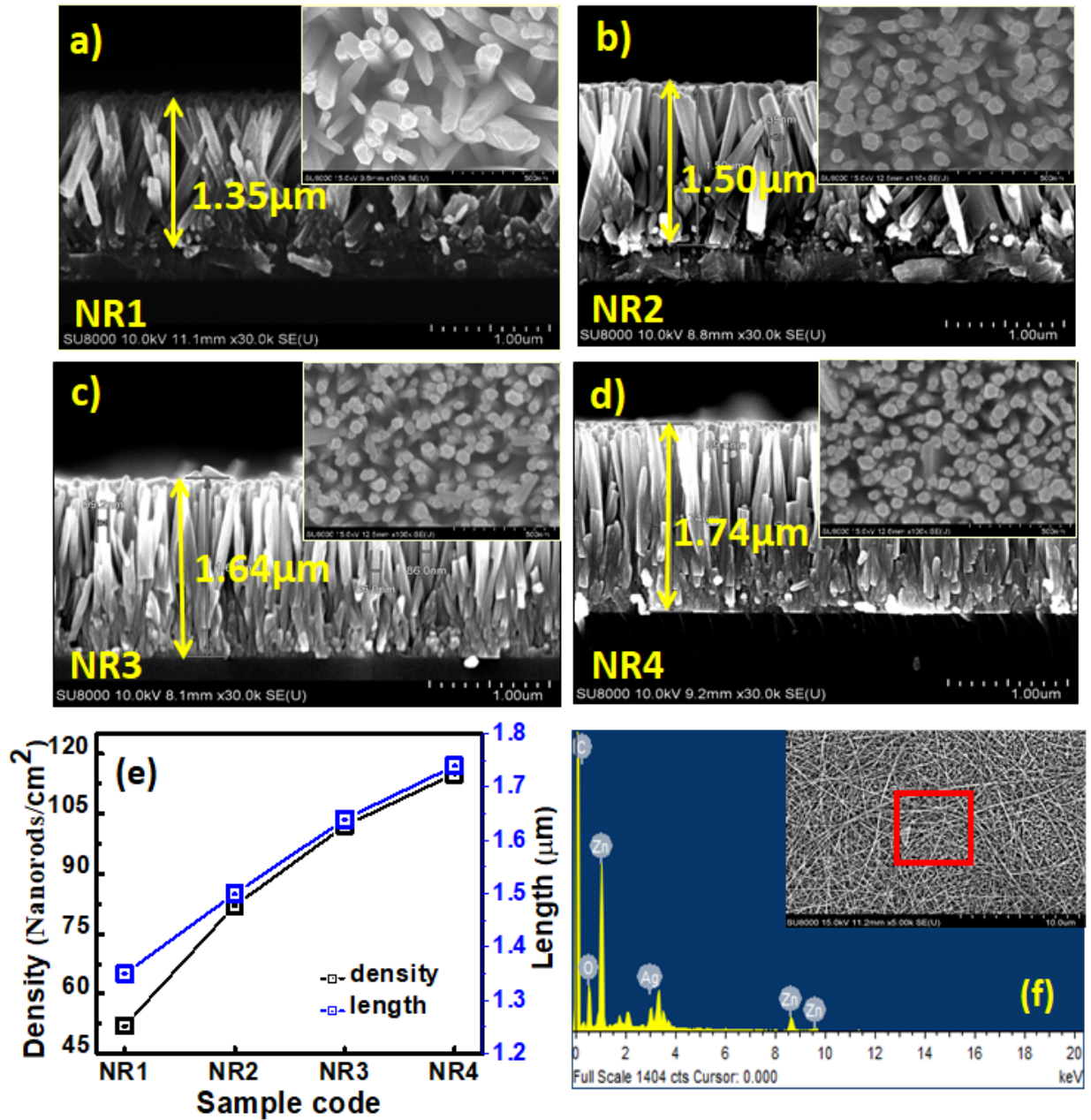
124

125 **Fig 2.** AFM surface topography of the seed layer deposited under an Ar–O₂ gas flow of (a) 30:00
 126 (pure Ar), (b) 20:10, (c) 10:20, and (d) 00:30 (pure O₂) scm. XRD pattern of (e) the deposited
 127 ZnO seed layer and (f) the ZnO-NRs. (g) (002) grain size of the seed layer and ZnO-NRs calculated
 128 from (e) and (f).

129

130 To further evaluate the microstructure of the NRs, an SEM analysis was conducted, and
 131 the results are displayed in Figs. 3(a)–3(e). EDX spectrum of the fabricated device is shown in Fig.
 132 3(f). That confirms the presence of all the metal oxide in the composite and quantitatively, as well
 133 as silver (Ag) presence is also observed, which is used as a top electrode. The SEM analysis affirms
 134 that all NRs are successfully grown vertically regardless of the various seed layer conditions. The
 135 top-view SEM images depict the decrease in the diameter of the NRs grown on the O-rich seed
 136 layer. This result corroborates with XRD analysis results (Fig. 2(g)). It was also found that the
 137 average length and the density of the NRs have a direct dependency on the seed layer condition.

138 The increase in the number of nucleation sites due to the higher surface roughness of the seed layer
 139 (Fig. 2(a)–2(d)) may induce this phenomenon [29,30]. An electrical test was conducted to
 140 investigate the sensing performance of the various NR structures.



141
 142 **Fig 3.** Cross-sectional SEM images of (a) NR1, (b) NR2, (c) NR3 (d) NR4. Insets in (a)–(d) display
 143 the top view of the NRs (e) Length and density of the ZnO-NRs grown on various seed layers and

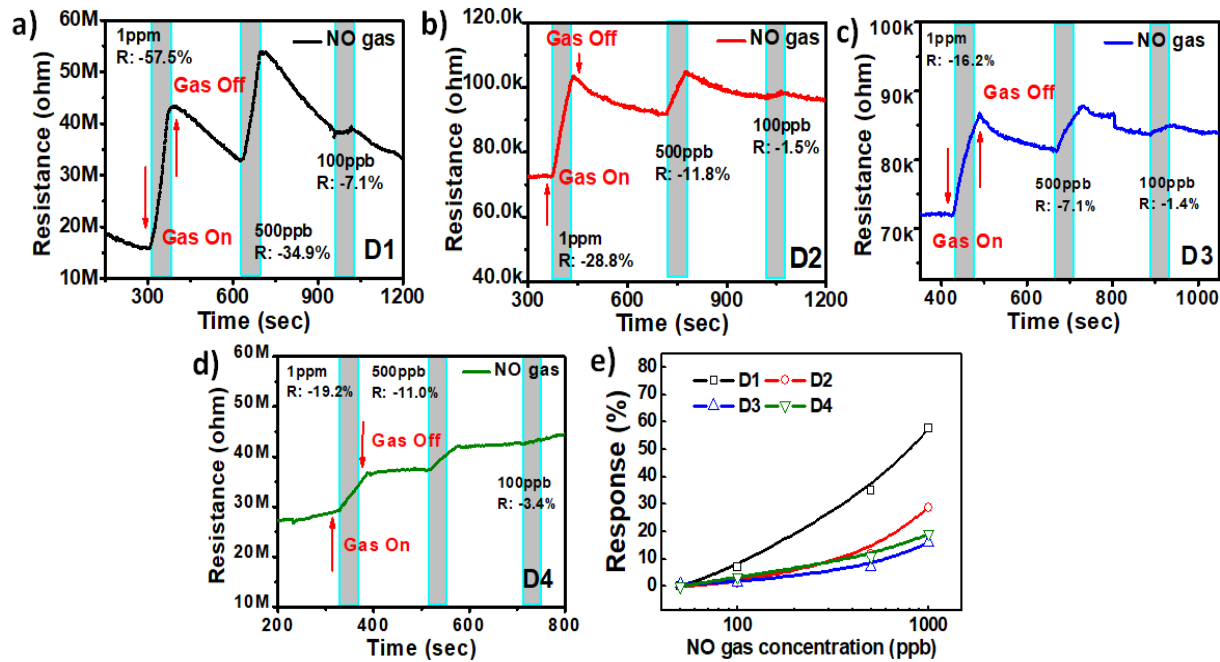
144 (f) EDX spectrum of the fabricated device (inset image represent the corresponding SEM of
145 mapping area).

146

147 **Gas sensing property**

148 The sensing performance of these various NR microstructures toward NO gas was then assessed.
149 Figures 4(a)–4(d) show the resistance (ohm) and time (sec) curves of the gas-sensing performance
150 of device D1, D2, D3, D4 and inset images shows I-V curves of the device, respectively. The gas-
151 sensing measurements were conducted at room temperature ($\sim 26^{\circ}\text{C}$) by employing a bias voltage
152 of 5 V, and the nitric oxide gas concentration was 100 ppb to 1 ppm. The calculated response is
153 denoted as R and presented in Figs. 4(a)–4(d), and the device response is summarized in Fig. 4(e).
154 The results reveal that from low to high concentration, there is an increment in the gas-sensing
155 response with respect to the NO gas. We found that the gas response of the device with NRs grown
156 on the seed layer made at pure Ar ambient(D1) is far superior than the response of all other devices.
157 The D1 sensor (fabricated on ZnO-SL-1) presents the highest response with values of 57.5%,
158 34.9%, and 7.1% at NO concentrations of 1 ppm, 500 ppb, and 100 ppb, respectively. On the other
159 hand, the response significantly decreases in the other devices (Fig. 4(e)). It is worth noting that
160 the four sensors' resistances are very different in air as shown in Fig. 4. We suggest the possible
161 reason that the variation of the pristine resistance of the devices is due to the conductivity of Ag
162 nanowires top electrode (TE). Since the TE was fabricated employing a drop coating technique,
163 thus, the actual weight of Ag onto the nanorods may slightly different in each drop. Consequently,
164 it may lead to varying amount of Ag nanowires in TE between devices and the resistance variation
165 of the devices. Nevertheless, the Ag(TE)/nanorods contact is following ohmic contact which may
166 not have significant role in the sensing mechanism. Under the comparison with other reported
167 sensors demonstrating good response toward NO gas, the sensing response of our sensors proposed

168 in this work is better than those made by several other methods and sensing materials listing in
 169 Table 1.



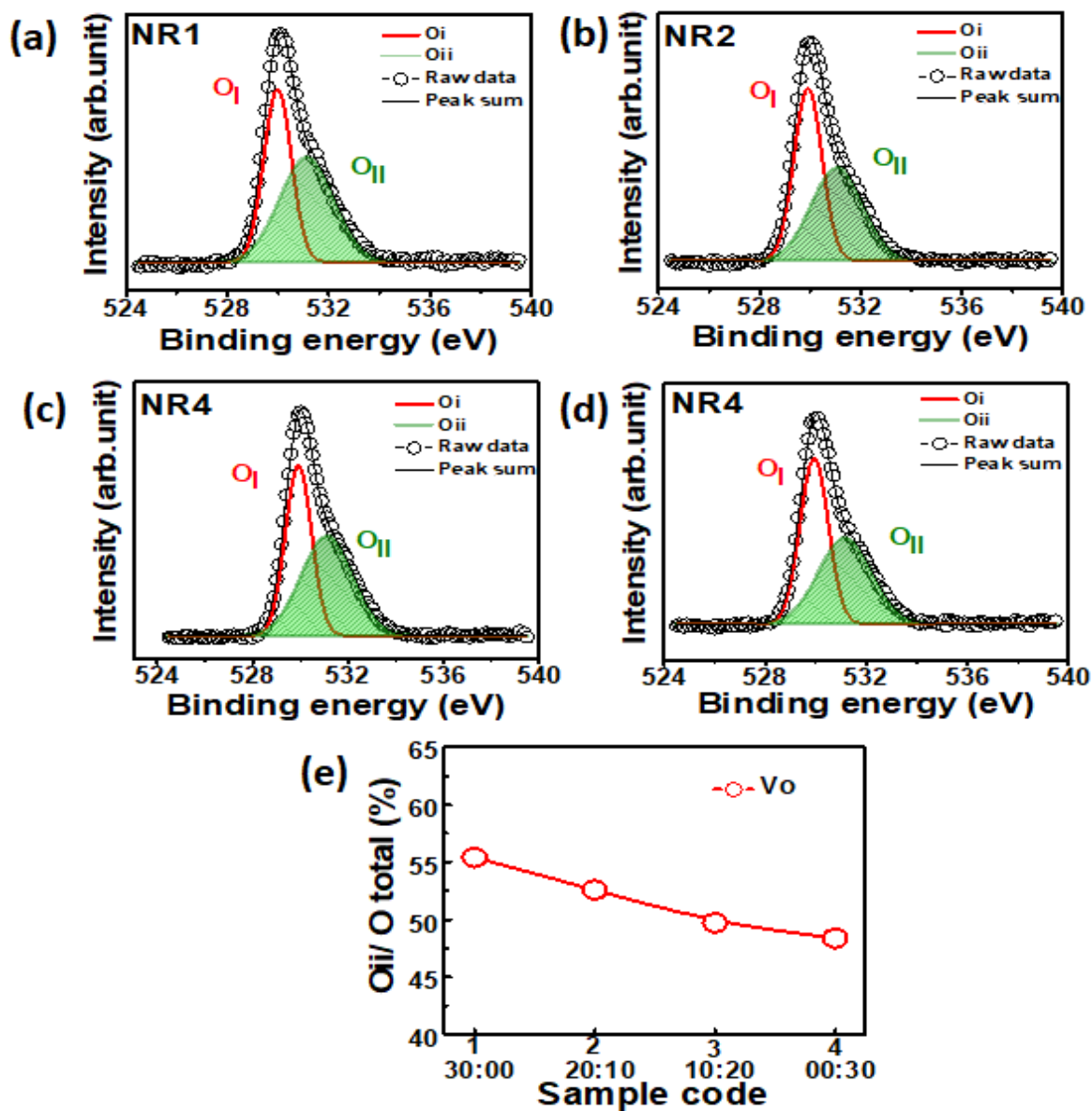
170
 171 **Fig 4.** Resistance- time curves of (a) D1, (b) D2, (c) D3, and (d) D4 devices and inset I-V results
 172 of (a) D1, (b) D2, (c) D3, and (d) D4 devices, respectively. (e) Gas-sensing response results of the
 173 various devices measured at room temperature.

174
 175 This result indicates that the property of the ZnO seed layer determines the microstructure
 176 of the NRs; thus, the property of the ZnO seed layer may significantly affect the sensing
 177 performance of the NRs. The seed layer has no sensing capability (data not shown), which
 178 indicates that the sensing behavior is only from the NR layer. Although the NRs grown on a seed
 179 layer deposited with a less amount of Ar gas have greater lengths, the sensing performance of such
 180 NRs tends to decrease. This finding suggests that the sensing performance does not always
 181 dependent on the height of the NRs, as is commonly observed [9,23]. Therefore, we conducted
 182 materials analysis to understand this phenomenon.

183
184
185
186
187
188
189
190
191
192
193
194
195
196
197
198
199

Chemical analysis (XPS)

Oxygen vacancy defects serve a significant role in ZnO-based sensor devices [31]. Figures 5 (a)–5(d) show the XPS analysis results of the O1s core level of the ZnO-NRs grown on various seed layers. The O1s spectra were fitted to two Gaussian-resolved peaks—a low binding energy peak (O_i) that corresponds to the O^{2-} ions on the hexagonal ZnO structure and a high binding energy peak (O_{ii}) that is attributed to the oxygen-deficient region (oxygen vacancy-rich region) and the chemisorbed or dissociate oxygen species on the surface of ZnO [32,33]. The concentration of oxygen vacancy V_o is represented by the O_{ii}/O_{Total} ratio [22], as depicted in Fig. 5(e). The ZnO-NRs grown on seed layers deposited with a higher Ar portion have a higher V_o concentration. This may be because a seed layer deposited at ambient conditions with a low amount of oxygen may contain a higher V_o concentration (data not shown). Moreover, the NRs prefer to grow in a condition that requires the lowest formation energy corresponding to the seed layer properties [34]. Therefore, we can assume that the NRs may grow based on the lattice condition of the seed layer to grow with the lowest energy.



200
 201 **Fig 5.** XPS spectra of the O1s core level of the ZnO-NRs grown on (a) SL1, (b) SL2, (c) SL3, and
 202 (d) SL4 films. (e) Oxygen vacancy concentration in the NRs.

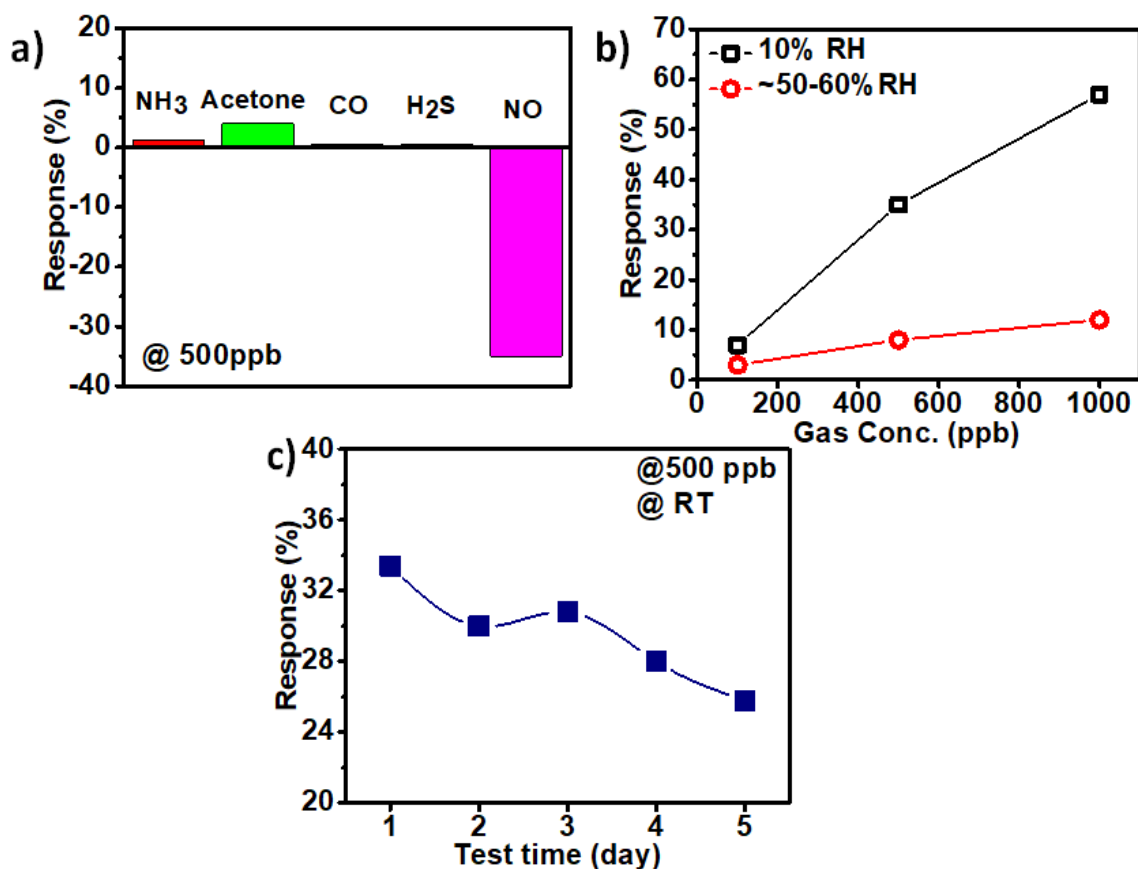
203
 204 **Selectivity and stability test for NO sensing**

205 Selectivity and stability are very essential parameters to check the performance of the gas sensor
 206 device. The Device D1 was fabricated to perform the selectivity and stability test. The gas

207 selectivity test was carried out by using NH₃, CO, H₂S and acetone gases and the results are
208 depicted in Fig 6(a). It is indicated that the fabricated sensors have no response to 500-ppb CO and
209 H₂S gases at room temperature. When detecting 500-ppb acetone and NH₃ for 30 sec, the sensors
210 are observed 4.6% and 1.2 % gas responses, respectively, as shown in Fig. 6(a). It is worth noting
211 that, the sensor exhibits a 34.9% sensing response when being exposed to 500-ppb NO indicating
212 that sensor can be selective in detection of NO from above mentioned gases at room temperature.

213 Furthermore, the effect of relative humidity on the gas sensing performance of the device
214 D1 was studied at room temperature and the results are depicted in Fig 6 (b). The sensing response
215 is decreased in high humidity (55-65% RH) environment due to absorption of water molecule from
216 the humidity atmosphere. This phenomenon reduces the absorption rate of NO molecule at the
217 sensing layer [35].

218 Sensor stability is also critical characteristic to be used in practical application. To
219 acknowledge the stability test, the device D1 was measured at 500-ppb NO gas under the same
220 test conditions as before for up to 5 days and the observed responses are 33.9, 30.6, 31.2, 28.2 and
221 26.0% as exhibited in Fig 6(c), indicating a small downward trend in gas response. Nevertheless,
222 the gas response is decreased just a few percent within 5 days confirming that the sensor has good
223 stability at room temperature.



224

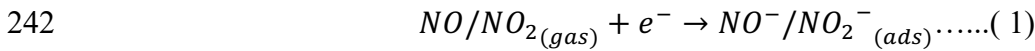
225 **Fig 6.** (a) The selectivity performance of the sensor to NH₃, acetone, CO and H₂S at room
 226 temperature, (b) Sensing response of Device D1 in high humidity environment (RH ~ 55-65 %)
 227 and (c) The D1 stability results up to 5 days.

228

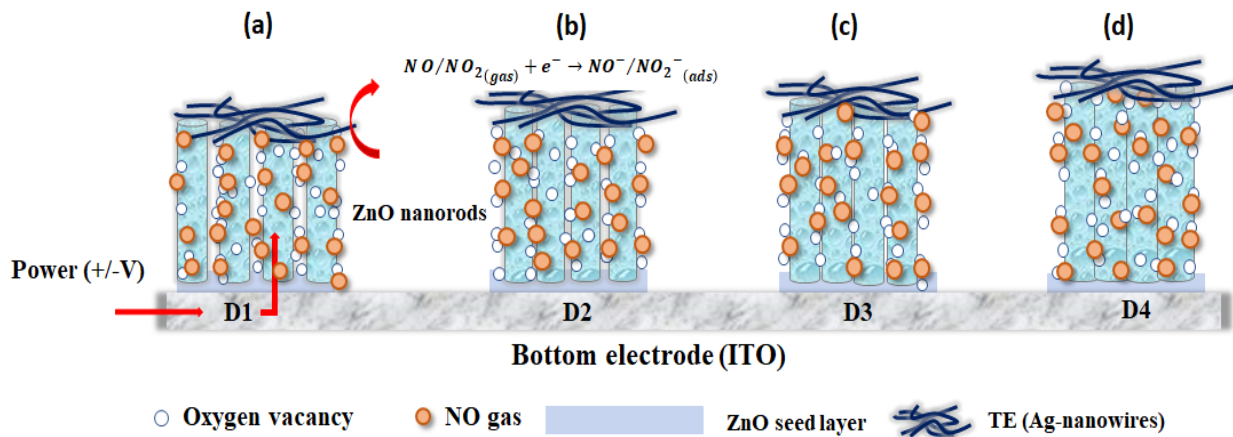
229 **Gas sensing mechanism**

230 The sensing mechanism of the various devices is proposed and depicted in Fig. 7. The sensing
 231 mechanism is based on the adsorption–desorption reaction of the gas molecules at the surface of
 232 the NRs. When the sensor is exposed to air, oxygen molecules are easily absorbed on the sensor
 233 surface and captures the electrons from conduction band. The gas sensor response varies due to
 234 different morphology structure and absorption rate at the sensing layer. After oxygen adsorption

235 process, a depletion layer is formed at the outer surface of sensing nanorods layer and results the
 236 higher resistance [36]. The reaction induces a change in the electrical property (conductivity or
 237 resistance) of the device. This change indicates a response toward the target gas [37]. As shown in
 238 Fig. 7, the introduction of NO gas (in an ambient of dry air as the background gas) to the sensor
 239 devices results in the adsorption of the NO molecules on the surfaces of the NRs. The NO
 240 molecules are ionized at the surface by capturing the electron from the ZnO. The formula of this
 241 reaction is as follows:



243 Hereafter, the $NO^- - NO_2^-(ads)$ reactant forms a depletion layer on the surface of the NRs. Thus,
 244 the electron concentration on the surface of the NRs decreases. This decrease results in an increase
 245 in the resistance of the devices [31]. The oxygen vacancy is an electron donor; therefore, the
 246 concentration of the oxygen vacancy influences the amount of NO absorbed on the surface of the
 247 NRs.



248
 249 **Fig 7.** Schematic of the gas sensor mechanism in (a) D1, (b) D2, (c) D3, and (d) D4 devices.

250

251 The NRs of the device D1 (Fig. 7(a)) exhibit a high oxygen vacancy concentration (Fig. 5(a)) with
252 a high openness structure (low density, Fig. 3(a)). These chemical and structural properties enable
253 the abundant absorption of NO on the surface of the NRs, thus inducing a high response toward
254 the gas target (Fig. 4(a)). Moreover, the NRs of the device D2 (Fig. 7(b)) have a lower oxygen
255 vacancy concentration (Fig. 5(b)) and higher density (Fig. 3(b)) than the NRs of the device D1.
256 Therefore, less NO molecules can be absorbed by the NRs of the device D2, which causes a lower
257 sensing response (Fig. 4(b)). Similarly, the NRs of the devices D3 and D4 (Fig. 7(c) and 7(d)) have
258 very low oxygen vacancy concentrations (Fig. 5(c) and 5(d)) and a low openness structure (Fig.
259 3(c) and 3(d)). Thus, the sensing response of these devices is significantly lower than the other
260 devices (Fig. 4(c) and 4(d)). However, the device D4 presents a slightly higher gas response than
261 that of the device D3 (Fig. 4(e)). We suggest that this behavior is attributed to the oxygen vacancy
262 concentration of NR4 is slightly lower than that of D3, but the length of NR4 is much longer than
263 that of NR3 (Figs. 3(c) and 3(d)). Thus, this condition helps to increase the area that can be exposed
264 to the NO molecules [21,38].

265

266 **Conclusions**

267 In conclusion, we investigated the influence of the seed layer on the gas response. The ZnO-NRs
268 that are grown on a seed layer deposited with a low amount of O₂ gas were found to be more
269 sensitive toward NO gas. The concentration of the oxygen vacancy defects and the microstructure
270 of the NRs determine the sensing performance. Although the NRs grown on a seed layer deposited
271 with a low amount of O₂ gas have a shorter length, the high oxygen vacancy concentration and the
272 loose structure of NRs provide high sensitivity. A sensing response superior than that provided by
273 several other methods can be achieved by simply adjusting the seed layer. It worth noting that the
274 devices require various times to recover the original condition (pristine resistance) after the

275 exposure to the gas. This phenomenon may be related to the surface area effect and the NO
276 releasing mechanism from the surface of the nanorods. It is very interesting to be explored in our
277 future investigation. Nevertheless, this study suggests that the property of the seed layer cannot be
278 overlooked when designing ZnO-NR-based sensor devices.

279

280 **Acknowledgment**

281 This work was supported by the Ministry of Science and Technology, Taiwan, under projects
282 MOST 105-2221-E-009-143-MY3 and MOST-107- 2633-E-009 -003.

283 **Conflicts of interest**

284 The authors declare no conflicts of interest.

285

286 **References**

- 287 [1] Wetchakun K, Samerjai T, Tamaekong N, Liewhiran C, Siriwong C, Kruefu V,
288 Wisitsoraat A, Tuantranont A and Phanichphant S 2011 Semiconducting metal oxides as
289 sensors for environmentally hazardous gases *Sensors Actuators, B Chem.* **160** 580–91
- 290 [2] Shehada N, Cancilla J C, Torrecilla J S, Pariente E S, Brönstrup G, Christiansen S,
291 Johnson D W, Leja M, Davies M P A, Liran O, Peled N and Haick H 2016 Silicon
292 Nanowire Sensors Enable Diagnosis of Patients via Exhaled Breath *ACS Nano* **10** 7047–
293 57
- 294 [3] Di Natale C, Paolesse R, Martinelli E and Capuano R 2014 Solid-state gas sensors for
295 breath analysis: A review *Anal. Chim. Acta* **824** 1–7
- 296 [4] Zhang S-L, Lim J-O, Huh J-S and Lee W 2012 Selective Growth of ZnO Nanorods and

- 297 Its Gas Sensor Application *IEEE Sens. J.* **12** 3143–8
- 298 [5] Öztürk S, Kiliç N and Öztürk Z Z 2013 Fabrication of ZnO nanorods for NO₂ sensor
299 applications: Effect of dimensions and electrode position *J. Alloys Compd.* **581** 196–201
- 300 [6] Zhu L and Zeng W 2017 Room-temperature gas sensing of ZnO-based gas sensor: A
301 review *Sensors Actuators A Phys.* **267** 242–61
- 302 [7] Galstyan V, Comini E, Ponzoni A, Sberveglieri V and Sberveglieri G 2016 ZnO Quasi-
303 1D Nanostructures: Synthesis, Modeling, and Properties for Applications in
304 Conductometric Chemical Sensors *Chemosensors* **4** 6
- 305 [8] Ganesh R S, Mani G K, Elayaraja R, Durgadevi E, Navaneethan M, Ponnusamy S,
306 Tsuchiya K, Muthamizhchelvan C and Hayakawa Y 2018 Surfactant free controllable
307 synthesis of 2D – 1D ZnO hierarchical nanostructure and its gas sensing properties *Appl.*
308 *Surf. Sci.* **449** 838–45
- 309 [9] Jagadale S B, Patil V L, Vanalakar S A, Patil P S and Deshmukh H P 2018 Preparation,
310 characterization of 1D ZnO nanorods and their gas sensing properties *Ceram. Int.* **44**
311 3333–40
- 312 [10] Wang M, Xing C, Cao K, Meng L and Liu J 2014 Alignment-controlled hydrothermal
313 growth of well-aligned ZnO nanorod arrays *J. Phys. Chem. Solids* **75** 808–17
- 314 [11] Simanjuntak F, Singh P, Chandrasekaran S, Lumbantoruan F J, Yang C-C, Huang C-J,
315 Lin C-C and Tseng T-Y 2017 Role of Nanorods Insertion Layer In ZnO-based
316 Electrochemical Metallization Memory Cell *Semicond. Sci. Technol.* 0–12
- 317 [12] Ganbavle V V., Inamdar S I, Agawane G L, Kim J H and Rajpure K Y 2016 *Synthesis of*
318 *fast response, highly sensitive and selective Ni:ZNO based NO₂ sensor* vol 286 (Elsevier
319 B.V.)

- 320 [13] Basyooni M A, Shaban M and El Sayed A M 2017 Enhanced Gas Sensing Properties of
321 Spin-coated Na-doped ZnO Nanostructured Films *Sci. Rep.* **7** 1–12
- 322 [14] Zhang B, Li M, Song Z, Kan H, Yu H, Liu Q, Zhang G and Liu H 2017 Sensitive H₂S
323 gas sensors employing colloidal zinc oxide quantum dots *Sensors Actuators, B Chem.* **249**
324 558–63
- 325 [15] Khojier K and Savaloni H 2015 Improving the H₂ Gas Sensitivity of ZnO Thin Films by
326 Modifying the Annealing Conditions *J. Electron. Mater.* **44** 3458–64
- 327 [16] da Silva L F, M’Peko J C, Catto A C, Bernardini S, Mastelaro V R, Aguir K, Ribeiro C
328 and Longo E 2017 UV-enhanced ozone gas sensing response of ZnO-SnO₂
329 heterojunctions at room temperature *Sensors Actuators, B Chem.* **240** 573–9
- 330 [17] Cheng J J, Nicaise S M, Berggren K K and Gradečak S 2016 Dimensional Tailoring of
331 Hydrothermally Grown Zinc Oxide Nanowire Arrays *Nano Lett.* **16** 753–9
- 332 [18] Azzez S A, Hassan Z, Hassan J J, Alimanesh M, Rasheed H S, Sabah F A and Abdulateef
333 S A 2016 Hydrothermal synthesis of highly crystalline ZnO nanorod arrays: Dependence
334 of morphology and alignment on growth conditions **020034** 020034
- 335 [19] Song J and Lim S 2007 Effect of seed layer on the growth of ZnO nanorods *J. Phys.*
336 *Chem. C* **111** 596–600
- 337 [20] Guillemin S, Consonni V, Appert E, Puyoo E, Rapenne L and Roussel H 2012 Critical
338 nucleation effects on the structural relationship between ZnO seed layer and nanowires *J.*
339 *Phys. Chem. C* **116** 25106–11
- 340 [21] Chang C J, Hung S T, Lin C K, Chen C Y and Kuo E H 2010 Selective growth of ZnO
341 nanorods for gas sensors using ink-jet printing and hydrothermal processes *Thin Solid*
342 *Films* **519** 1693–8

- 343 [22] Singh P, Simanjuntak F M, Kumar A and Tseng T 2018 Resistive switching behavior of
344 Ga doped ZnO-nanorods film conductive bridge random access memory *Thin Solid Films*
345 **660** 828–33
- 346 [23] Singh P, Hu L-L, Zan H-W and Tseng T-Y 2019 Highly sensitive nitric oxide gas sensor
347 based on ZnO-nanorods vertical resistor operated at room temperature *Nanotechnology* **30**
348 095501
- 349 [24] Zhang J P, He G, Zhu L Q, Liu M, Pan S S and Zhang L D 2007 Effect of oxygen partial
350 pressure on the structural and optical properties of ZnO film deposited by reactive
351 sputtering *Appl. Surf. Sci.* **253** 9414–21
- 352 [25] Bai S N and Wu S C 2011 Synthesis of ZnO nanowires by the hydrothermal method,
353 using sol-gel prepared ZnO seed films *J. Mater. Sci. Mater. Electron.* **22** 339–44
- 354 [26] Cullity B D and Stock S R 2001 *Elements of X-ray Diffraction* (Prentice Hall)
- 355 [27] Huang H-W, Kang C-F, Lai F-I, He J-H, Lin S-J and Chueh Y-L 2013 Stability scheme
356 of ZnO-thin film resistive switching memory: influence of defects by controllable oxygen
357 pressure ratio. *Nanoscale Res. Lett.* **8** 483
- 358 [28] Lee J-B, Park C-K and Park J-S 2009 Physical Properties of RF-Sputtered ZnO Thin
359 Films: Effects of Two-Step Deposition *J. Korean Phys. Soc.* **50** 1073
- 360 [29] Tien L and Chen Y 2012 Applied Surface Science Effect of surface roughness on
361 nucleation and growth of vanadium pentoxide nanowires *Appl. Surf. Sci.* **258** 3584–8
- 362 [30] Tong Y, Liu Y, Dong L, Zhao D, Zhang J, Lu Y, Shen D and Fan X 2006 Growth of ZnO
363 nanostructures with different morphologies by using hydrothermal technique *J. Phys.*
364 *Chem. B* **110** 20263–7

- 365 [31] Kaur M, Kailasaganapathi S, Ramgir N, Datta N, Kumar S, Debnath A K, Aswal D K and
366 Gupta S K 2017 Gas dependent sensing mechanism in ZnO nanobelt sensor *Appl. Surf.*
367 *Sci.* **394** 258–66
- 368 [32] Kim W, Choi M and Yong K 2015 Generation of oxygen vacancies in ZnO
369 nanorods/films and their effects on gas sensing properties *Sensors Actuators B Chem.* **209**
370 989–96
- 371 [33] Simanjuntak F M, Ohno T and Samukawa S 2019 Neutral Oxygen Beam Treated ZnO-
372 Based Resistive Switching Memory Device *ACS Appl. Electron. Mater.* acsaelm.8b00055
- 373 [34] Yuan K, Yin X, Li J, Wu J, Wang Y and Huang F 2010 Preparation and DSC application
374 of the size-tuned ZnO nanoarrays *J. Alloys Compd.* **489** 694–9
- 375 [35] Agarwal S, Rai P, Navarrete E, Llobet E and Güell F 2019 Sensors and Actuators B :
376 Chemical Gas sensing properties of ZnO nanostructures (flowers / rods) synthesized by
377 hydrothermal method **292** 24–31
- 378 [36] Harale N S, Dalavi D S, Mali S S, Tarwal N L, Vanalakar S A, Rao V K, Hong C K, Kim
379 J H and Patil P S 2018 Single-step hydrothermally grown nanosheet-assembled tungsten
380 oxide thin films for sensitive and selective NO₂ gas detection *J. Mater. Sci.* **53** 6094–105
- 381 [37] Zhang X, Qin J, Xue Y, Yu P, Zhang B, Wang L and Liu R 2014 Effect of aspect ratio
382 and surface defects on the photocatalytic activity of ZnO nanorods *Sci. Rep.* **4** 4–11
- 383 [38] Liu F T, Gao S F, Pei S K, Tseng S C and Liu C H J 2009 ZnO nanorod gas sensor for
384 NO₂ detection *J. Taiwan Inst. Chem. Eng.* **40** 528–32
- 385 [39] Lin C H, Chang S J and Hsueh T J 2017 A WO₃nanoparticles NO gas sensor prepared by
386 hot-wire CVD *IEEE Electron Device Lett.* **38** 266–9

- 387 [40] Kim C-Y, Jung H, Choi H and Choi D 2016 Synthesis of one-dimensional SnO₂ lines by
388 using electrohydrodynamic jet printing for a NO gas sensor *J. Korean Phys. Soc.* **68** 357–
389 62
- 390 [41] Lin C Y, Fang Y Y, Lin C W, Tunney J J and Ho K C 2010 Fabrication of NO_x gas
391 sensors using In₂O₃-ZnO composite films *Sensors Actuators, B Chem.* **146** 28–34
- 392 [42] Liu B, Liu X, Yuan Z, Jiang Y, Su Y, Ma J and Tai H 2019 A flexible NO₂ gas sensor
393 based on polypyrrole/nitrogen-doped multiwall carbon nanotube operating at room
394 temperature *Sensors Actuators, B Chem.* **295** 86–92
- 395 [43] Zhang Z, haq M, Wen Z, Ye Z and Zhu L 2018 Ultrasensitive ppb-level NO₂ gas sensor
396 based on WO₃ hollow nanosphers doped with Fe *Appl. Surf. Sci.* **434** 891–7
- 397 [44] Soltabayev B, Er I K, Surel H, Coşkun A, Yildirim M A, Ateş A and Acar S 2019
398 Influence of Ni doping on the nitric oxide gas sensing properties of Zn_{1-x}Ni_xO thin films
399 synthesized by silar method *Mater. Res. Express* **6**
- 400 [45] Samanta C, Ghatak A, Raychaudhuri A K and Ghosh B 2019 ZnO/Si nanowires
401 heterojunction array-based nitric oxide (NO) gas sensor with noise-limited detectivity
402 approaching 10 ppb *Nanotechnology* **30** 305501
- 403 [46] Gupta S K, Joshi A and Manmeet K 2010 Development of gas sensors using ZnO
404 nanostructures *J. Chem. Sci.* **122** 57–62
- 405 [47] Singh G, Choudhary A, Haranath D, Joshi A G, Singh N, Singh S and Pasricha R 2012
406 ZnO decorated luminescent graphene as a potential gas sensor at room temperature
407 *Carbon N. Y.* **50** 385–94

408 **Table Caption**

409 Table 1. Performance comparisons of the NO gas sensors between those from published papers
410 and that of present study.

411

412

413

414

415

416

417

418

419

420

421

422

423

424

425

426

427

428 **Table 1.**

Sensing material	Operating Temp.	Sensing Response (%)	Conc. (ppm)	Reference
WO ₃ Nanoparticles	150°C	~16	0.35	[39]
SnO ₂ line patterns	300°C	~32	20	[40]
In ₂ O ₃ -ZnO composite film	150°C	38	7.8	[41]
N ₂ +MWCNT	350°C	24.8	5	[42]
Fe+ WO ₃ nanosphers	120°C	4.7	1	[43]
Zn _{1-x} Ni _x O thin film	95°C	65	25	[44]
ZnO/p-Si NWs	Room temp.	35	10	[45]
ZnO nanowires	Room temp.	40	1	[46]
ZnO-GrO nanocomposite	Room temp.	25	5	[47]
ZnO-NRs thin film	Room temp.	57.5	1	This work

429